

Influence of operating conditions and cathode parameters on desalination performance of hybrid CDI systems

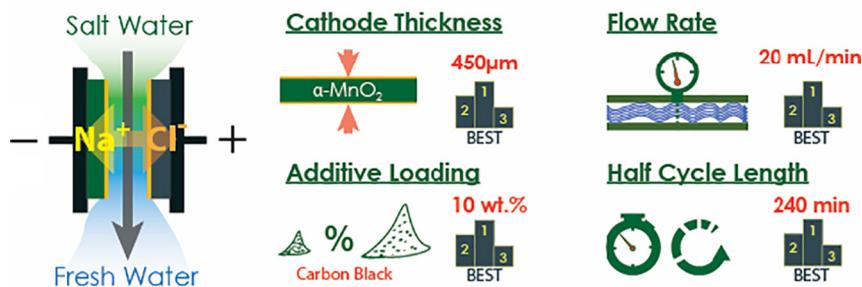
Lutfi Agartan^a, Brendan Hayes-Oberst^b, Bryan W. Byles^b, Bilen Akuzum^a, Ekaterina Pomerantseva^b, E. Caglan Kumbur^{a,*}

^a *Electrochemical Energy Systems Laboratory, Department of Mechanical Engineering and Mechanics, Drexel University, Philadelphia, PA 19104, USA*

^b *Materials Electrochemistry Laboratory, Department of Materials Science and Engineering, Drexel University, Philadelphia, PA 19104, USA*

GRAPHICAL ABSTRACT

Parametric Study of Hybrid CDI Systems



ARTICLE INFO

Keywords:

$\alpha\text{-MnO}_2$ nanowires
Electrosorption kinetics
Hybrid capacitive deionization
In-situ SAR vs SAC plot
Water desalination

ABSTRACT

The objective of this study is to understand the effects of operating conditions and cathode parameters on the salt removal performance of hybrid capacitive deionization systems (HCDI). Hence, the effects of half cycle length, flow rate, cathode thickness, and conductive additive loading in the cathode are systematically investigated. Hydrothermally synthesized $\alpha\text{-MnO}_2$ was selected as the active material in the cathode. Desalination results indicate notable dependence of HCDI performance on the investigated parameters. For instance, increasing half cycle length increases the salt adsorption capacity (SAC) by ~58% but decreases the peak salt adsorption rate (PSAR) by ~28%. On the other hand, increasing the flow rate leads to an increase of the SAC and PSAR by ~25% and ~115%, respectively. Increase in the cathode thickness also showed a notable decay in performance with 43% drop in SAC. The amount of conductive additive in the cathode was also investigated to observe the impact of electrical conductivity on the CDI performance. Salt adsorption capacity and rate of HCDI systems containing identical active materials show strong dependence on the operation conditions and cathode parameters, which suggests a necessity of developing an understanding of the impact of these conditions on the system performance.

* Corresponding author.

E-mail address: eck32@drexel.edu (E. Caglan Kumbur).

1. Introduction

Capacitive deionization (CDI) has attracted significant attention for water treatment applications due to its lower cost and higher energy efficiency compared to current desalination methods such as reverse osmosis or distillation [1–3]. Typically, CDI cells utilize carbon electrodes that, when polarized by a constant potential or current, remove ions from solution via electric double layer storage on the surface of the electrodes [1–3]. When the potential or current is removed or reversed, ions are released back into solution, regenerating the electrodes for subsequent salt removal. The salt adsorption capacity and charge efficiency of a CDI system can be improved through inclusion of ion exchange membranes in a cell architecture known as membrane CDI (MCDI), where the ion exchange membranes prevent co-ion expulsion and enhance charge efficiency [4,5]. However, the salt adsorption capacity of MCDI systems is still limited by the intrinsically low capacity of the carbon electrodes and must be further improved for CDI technology to advance as a viable desalination method [3].

Recent work has shown that the salt adsorption capacity of a CDI cell can be increased significantly through replacing one of the carbon electrodes with a redox active electrode in an approach known as hybrid CDI (HCDI) [6]. In this approach, the redox active electrode removes ions from solution via a charge-transfer process involving intercalation of the ions from solution into the active material's crystal structure. A greater volume of the active material can be utilized, and thus salt adsorption capacity is no longer limited by the available surface area of the active material in the electrode [7]. As a result, HCDI systems demonstrate superior salt removal performance when compared to MCDI systems. For example, a $\text{Na}_{0.44}\text{MnO}_2$ /carbon black HCDI system has demonstrated a salt adsorption capacity of 31.2 mg g^{-1} , compared to 22.4 mg g^{-1} for an MCDI cell [6]. In an effort to maximize the salt adsorption capacity of HCDI systems, several Faradaic electrode materials and composite electrodes have been investigated [8,9], including manganese oxides [6,8], Prussian blue nanoparticles [10], sodium iron pyrophosphate [11], molybdenum disulfide [12], vanadium oxide/multi-walled carbon nanotube composite [13], carbon/ MnO_2 composites [14,15], and Ag-coated carbon composite [16]. Furthermore, CDI cells containing redox-active or physical intercalation electrodes (i.e. MXene vs. MXene [17], Ag/AgCl vs MnO_2 [18], MoS_2 /CNT vs MoS_2 /CNT [19], $\text{Na}_{0.44}\text{MnO}_2$ vs. $\text{Na}_{0.44}\text{MnO}_2$ [20], and desalination battery CuHCF vs. CuHCF [21]) have been studied to improve salt removal performance.

Along with the development of novel materials for improving the performance of HCDI systems, we believe that a thorough understanding of the operational conditions and their effects on the performance would be beneficial in guiding the development efforts and the standardization of the testing framework for easier comparison of studies conducted by different groups worldwide, as Hawks, et al. suggested in their recent work [22]. Key differences in material properties between traditional porous carbon electrodes and redox active electrodes, such as electronic conductivity, surface area, and ion removal mechanism, necessitate the development of an understanding of the relationship between experimental parameters and desalination performance in an HCDI system. Although various cell designs are proposed for these systems, one can still agree upon universal operating and design parameters such as half cycle length, flow rate, and electrode thickness and composition, which can be easily cross-compared between different systems. Investigating the effects of such parameters on the CDI performance can greatly help in understanding the strengths and drawbacks of a certain CDI system and provide insights into further development. A similar systematic approach has already been reported for the MCDI configurations [23–25] and provided useful insights into effects of membrane presence to the CDI performance. In addition to the parameters investigated in this study, salt removal performance of an HCDI system also depends on other cell design parameters (i.e. shape and arrangement of the electrodes etc.), which are not altered in this

study.

Motivated by this, we present the effects of the several experimental parameters on the salt removal performance of an HCDI system containing a tunnel manganese oxide phase, $\alpha\text{-MnO}_2$, as the cathode and activated carbon cloth (ACC) as the anode. Specifically, the goal of this study is to understand the influence of experimental testing and design parameters on the salt removal performance of an HCDI system. Manganese oxide is chosen because it is an environmentally friendly, low cost and abundant material that is an excellent candidate for water desalination via HCDI [26]. $\alpha\text{-MnO}_2$ has been shown to exhibit promising performance as a cathode in NaCl , KCl , and MgCl_2 solutions for HCDI systems [8]. Here, we explore the effects of the half cycle length, flow rate, cathode thickness and conductive additive loading in a cathode on its salt removal performance.

2. Experimental procedure

2.1. Materials synthesis

$\alpha\text{-MnO}_2$ nanowires are prepared via hydrothermal synthesis following a previous report [27]. In a typical synthesis 632 mg of KMnO_4 (Acros Organics) and 216 mg of NH_4Cl (Strem Chemicals) are dissolved in 200 mL of distilled deionized (DI) water. 20 mL of this solution is added into a 23 mL Teflon-lined stainless-steel autoclave (Parr Instruments) and hydrothermally treated at 150 °C for 50 h. The product is then filtered and washed with approximately 1 L of distilled DI water, followed by drying at 100 °C for 24 h. The produced $\alpha\text{-MnO}_2$ nanowires are ground using an agate mortar and pestle for 30 min in preparation for electrode fabrication.

2.2. Electrode fabrication

All cathodes are prepared using the same method. The grounded $\alpha\text{-MnO}_2$ nanowires, carbon black (CB, Alfa Aesar), and polytetrafluoroethylene (PTFE, Sigma Aldrich) are mixed in ethanol (Acros Organics) in desired weight ratios with $\alpha\text{-MnO}_2$ and carbon black amounts varying and PTFE remaining constant at 5 wt%. Cathodes are then rolled to the desired thicknesses of 150, 300, 450, and 600 μm and cut to a square dimension of 3.16 cm × 3.16 cm, followed by drying at 100 °C for 24 h. Zorflex FM50K activated carbon cloth (ACC, Charcoal House LLC.) having 500 μm thickness is used as anode. ACC anodes are cut to the desired dimensions (3.16 cm × 3.16 cm) using a laser cutter (Full Spectrum Laser H-Series 4th Gen).

Masses of the anode and cathode were measured separately using a precision scale having 100 μg sensitivity. Volumes of electrodes were estimated via multiplying the thickness of the electrodes with the active areas of the electrodes. The thicknesses of the electrodes were measured using a micrometer, and their areas were set to 10 cm^2 . Densities of the electrodes were calculated by dividing the measured anode mass to the calculated anode volume and measured cathode mass to the calculated cathode volume. Calculated density values for cathodes and anodes having different thicknesses were given in Table 1.

Table 1
The anode, the cathode, and the total mass of the electrodes.

Thickness (μm)	Cathode mass (g)	Anode mass (g)	Total mass (g)	Cathode density (g/ cm^3)	Anode density (g/ cm^3)
150	0.205	0.146	0.351	1.36	0.29
300	0.296	0.139	0.435	0.99	0.28
450	0.430	0.155	0.585	0.96	0.31
600	0.612	0.168	0.780	1.02	0.34

2.3. Materials characterization

The morphology of the α -MnO₂ nanowires is characterized using scanning electron microscopy (SEM) on a Zeiss Supra 50VP (Germany). The energy dispersive X-ray spectroscopy (EDX) attachment on the SEM is used to determine the chemical composition of α -MnO₂ nanowires by averaging EDX spectra from multiple 10 μm by 10 μm regions. X-ray powder diffraction (XRD) for phase analysis is performed using a Rigaku SmartLab X-ray diffractometer (Japan) with Cu-K α radiation ($\lambda = 1.54056 \text{ \AA}$), a graphite monochromator, step size of 0.02°, and step time of 5 s. Cylindrical four-point probe having proper spacing of 1.00 mm (ResTest v1, Jandel Engineering Ltd., United Kingdom) is used for the electronic conductivity measurements of the cathodes while 10 μA of current is applied.

2.4. HCDI performance test

The HCDI cell (see Fig. S.1) contains graphite current collectors, α -MnO₂ as the cathode (see Section 2.2), ACC (Zorflex FM50K, 500 μm) as the anode, and ion exchange membranes (ASV, 120 μm and CSO, 100 μm , AGC Engineering Co.). The active electrode area of the HCDI cell is 10 cm^2 .

Desalination tests are conducted in batch mode configuration using a fresh 100 mL of 10 mM sodium chloride (NaCl) solution in each test. The solution is circulated through the cell using a peristaltic pump (MasterFlex L/S Precision Variable-Speed, MK-07557-10). The ionic conductivity of the NaCl solution is measured and recorded with an ionic conductivity meter (Mettler Toledo, S470 SevenExcellence) each 10 s. The HCDI cell is cycled between 1.2 V for charging and -1.2 V for discharging, using a Biologic VMP3 potentiostat (France).

To understand the influence of operation conditions and cathode thickness/composition on the performance of the HCDI system, different half cycle lengths (15, 30, 60, 120, and 240 mins), flow rates (5, 10, 20, and 40 mL min^{-1}), cathode thicknesses (150, 300, 450, and 600 μm), and conductive additive loading in a cathode (10, 30, 50, and 95 wt%) are investigated (see Fig. 1). Here, half cycle length refers to the time allotted for ion removal/release at $+1.2 \text{ V}/-1.2 \text{ V}$, respectively. Prior to each desalination test, setup is cycled between salt removal and release several times until a dynamic steady state is reached [28]. Salt adsorption capacity (SAC) and salt adsorption rate (SAR) are calculated from recorded ion concentration data. SAC and SAR are used to describe the salt adsorption capacity and rate of salt adsorption since such nomenclature is commonly used in the CDI community. However, this does not mean that salt removal occurs just by EDL adsorption. Rather, redox processes occur on the manganese oxide cathode and ions are stored electrostatically in the EDL on the carbon anode [8]. SAC of the HCDI system is calculated using Eq. (1).

$$\text{SAC} (\text{mg}_{\text{NaCl}} \text{ g}_{\text{electrode}}^{-1}) = \frac{\Delta C \cdot V \cdot \text{MW}_{\text{NaCl}}}{m} \quad (1)$$

where ΔC stands for the concentration change (M), V is the volume (L) of the saline solution, MW_{NaCl} is the molecular weight of NaCl (58.44 g mol⁻¹), and m is the total mass of the electrodes (g). SAR versus SAC are graphed for kinetic analyses of desalination half cycle. SAR is calculated from the ion concentration vs time data using Eq. (2) [23].

$$\text{SAR} (\text{mg}_{\text{NaCl}} \text{ g}_{\text{electrode}}^{-1} \text{ min}^{-1}) = \frac{\Delta C \cdot V \cdot \text{MW}_{\text{NaCl}}}{m \cdot t} \quad (2)$$

where t stands for the time (min).

3. Results & discussion

3.1. Materials characterization

Fig. S2a shows the flexible, high aspect ratio nanowire morphology of the synthesized α -MnO₂ powder. The diameter of the nanowires ranges from 50 to 100 nm, with lengths up to tens of micrometers. The chemical composition of the material is evaluated via EDX spectra (see Fig. S2a, inset) and determined to be $\text{K}_{0.11}\text{MnO}_2$. The diffraction pattern recorded for the α -MnO₂ nanowires, shown in Fig. S2b, reveals that the nanowires are highly crystalline with no impurities present and can readily be indexed to JCPDS #44-041 with I4/m space group. A schematic of the *ab* plane of the 2×2 octahedra tunnel structure is shown as the inset in Fig. S2b. K⁺ ions stabilize the structural tunnels of the material [29,30]. Since K⁺ ions are present in a relatively small amount within the material, the structural tunnels in α -MnO₂ provide ample volume for ion insertion, thus making α -MnO₂ an attractive material for electrochemical water desalination [8].

3.2. Effects of half cycle length on HCDI performance

The salt removal performance of HCDI systems can be limited by slow ion transport. It is important to make sure that the amount of time given for charging and discharging half cycles are long enough to let diffusion-limited processes occur but short enough to keep the system energy efficient. To do so, initially the effects of half cycle lengths on salt removal performance of an HCDI system are investigated. Fig. 2a shows the concentration vs time plots for different half cycle lengths for the HCDI setup containing a 150 μm thick MnO₂ cathode (85 wt% α -MnO₂, 10 wt% CB, 5 wt% PTFE) and a 500 μm thick ACC anode under 20 mL min^{-1} flow rate. For this task half cycle lengths of 15, 30, 60, 120, 240 mins are tested and the salt adsorption capacities (SAC) are calculated to be 16.3, 18.8, 20.0, 22.8, and 25.8 mg g^{-1} , respectively. These results suggest that with increasing half cycle length, SAC of the system increases with a nonlinear trend. Yet, it should be noted that for

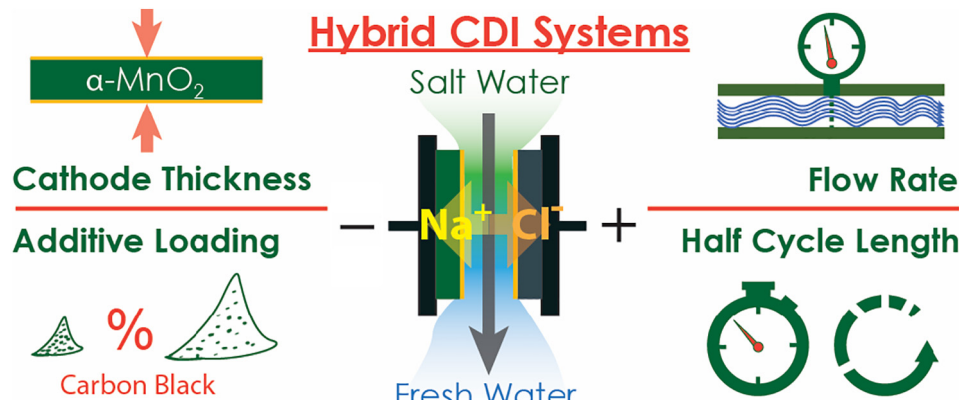


Fig. 1. The pictogram of the flow-by HCDI setup and studied operating conditions and cathode parameters.

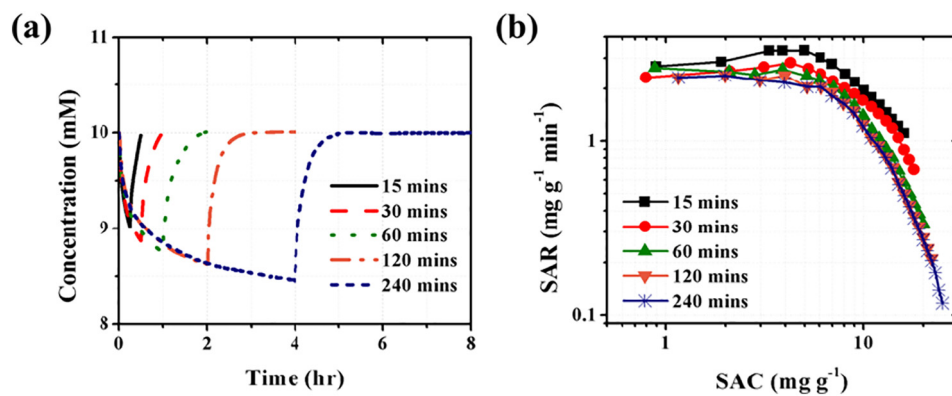


Fig. 2. (a) Concentration vs time graph, (b) in-situ SAR vs SAC plot of the HCDI depending on half cycle length.

the half cycles of 15, 30, and 60 min, ion concentrations have not approached to an asymptotic value (see Fig. 2a), indicating that the electrodes have not reached the saturated state by the end of the charging half cycles. Therefore, the active mass of the electrodes is believed to be underutilized for salt removal in these cases.

On the contrary, for 120 and 240 min long half cycles, the ion concentration vs. time curves approach an asymptotic value, meaning electrodes have reached the saturated state. Furthermore, increasing the half cycle length decreases the initial salt adsorption rate of the electrodes slightly, likely due to the higher state of saturation. As the half cycle length increases, ions are believed to penetrate deeper in the tunnel structure of the α -MnO₂, leading to higher SAC values. After several cycles of charging and discharging with longer half cycle lengths (until dynamic steady state is reached), electrodes are observed to adapt themselves to adsorb more ions at the expense of slower adsorption kinetics.

The In-situ SAR vs SAC plots of the HCDI system for the varying half cycle lengths are given in the Fig. 2b. As the half cycle length increases, the SAR values are observed to decrease for any selected SAC value on the In-situ SAR vs SAC plot. Furthermore, the In-situ SAR vs SAC plots of the HCDI system show slightly different behavior compared to that of the traditional CDI system where porous carbon electrodes are used in a symmetric setup. The In-situ SAR vs SAC plots of traditional CDI systems show initial increase followed by decrease at the SAR values with increasing SAC, without any plateau region [31,32]. However, the HCDI system shows initially high and steady (plateau) SAR value, which is believed to result from the faradaic electrode providing steady reaction rate while removing ions. Then, SAR values show a sharp decrease as the electrodes get closer to saturated state with increasing SAC value.

There are two active mechanisms of salt removal present in tunnel manganese oxides, such as α -MnO₂ [8]. The first mechanism is fast

absorption of ions from the solution through surface adsorption reaction, also known as pseudo-capacitance. This is indicated by the initial sharp decrease in concentration in Fig. 2a. After the fast absorption reaction, adsorbed cations begin to diffuse through the tunnels in the crystal structure of α -MnO₂ utilizing material volume via the second mechanism, which is the intercalation of ions [7]. In other words, active surface area used for ion adsorption is expected to be the same for whole charging period. The high plateau region of SAR values seen for HCDI is believed to correspond to the surface adsorption reactions occurring at a constant rate while charging. The rate decrease observed after the plateau region (Fig. 2b) is believed to be related to the electrodes not being able to adsorb more ions because of either the ACC surface getting saturated or ions not being able to penetrate through tunnels of α -MnO₂ due to them getting saturated. The SAR values corresponding to half cycle lengths of 120 and 240 mins converge after the plateau region, likely due to complete saturation of the tunnels of α -MnO₂ and after which the diffusion limited intercalation starts to determine the adsorption rate through the latter part of the charging. These findings highlight that having access to higher amount of active α -MnO₂ surface will enable faster kinetics with higher plateau SAR values. Due to 120 min long half cycle case reaching complete electrode saturation with comparable SAC and better SAR than that corresponding to 240 mins long half cycle, investigation of the impacts of flow rate, cathode thickness, and conductive additive loading in cathode on salt removal performance of the HCDI systems are conducted with the half cycle length of 120 mins.

3.3. Effects of flow rate on the HCDI performance

Fig. 3a shows the ion concentration vs time plots for the investigated flow rates. These experiments are conducted using a 150 μ m thick MnO₂ cathode (85 wt% α -MnO₂, 10 wt% CB, and 5 wt% PTFE), a

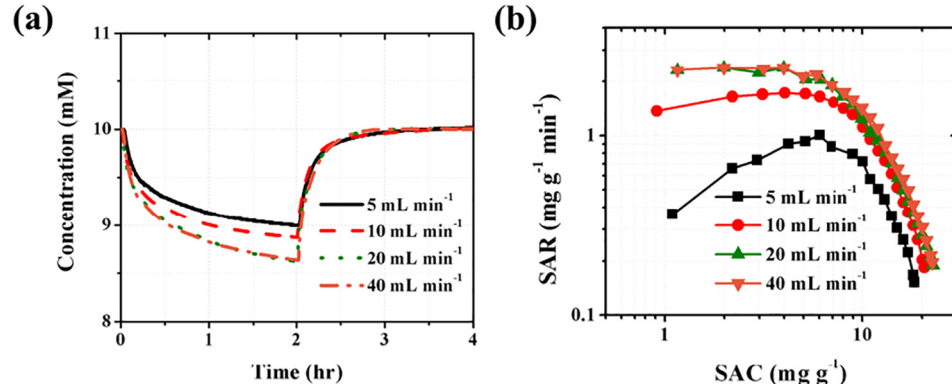


Fig. 3. (a) Concentration vs time graph, (b) in-situ SAR vs SAC plot of the HCDI depending on flow rate of the water.

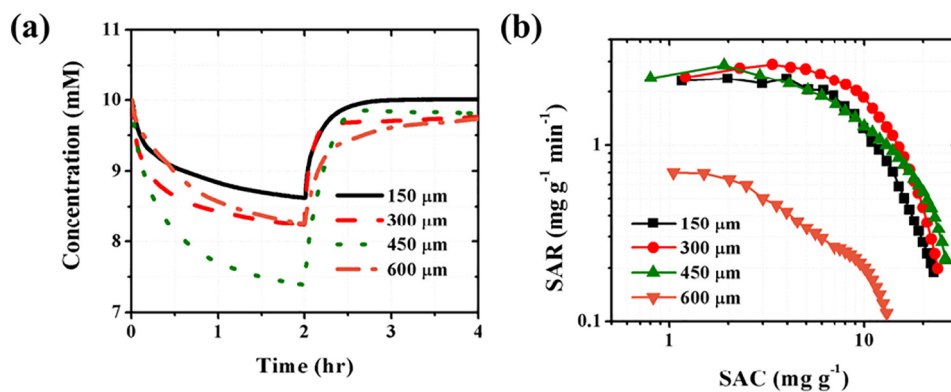


Fig. 4. (a) Concentration vs time graph, (b) in-situ SAR vs SAC plot of the HCDI depending on cathode thickness.

500 μm thick ACC anode, and 120 min long half cycle. Increasing flow rate leads to shorter residence time for the unit volume of saline water inside the HCDI cell, which results in shorter time for the Na^+ and Cl^- ions in solution to migrate towards the electrodes. This has been expected to lead to ion transport limitations and decrease both the SAC and the SAR of the HCDI systems, as in traditional CDI systems [23,32,33]. Yet, the SAC and the SAR trends observed for the HCDI system have deviated from that of traditional CDI system [23,33] towards the trend of redox flow battery (RFB) systems [34]. Upon systematically increasing the flow rate, a continuous increase in the SAC and the SAR of the HCDI system are observed. Electrodes employed for the 5, 10, 20, and 40 mL min^{-1} flow rates have reached saturated state and achieved the SAC values of 18.3, 20.5, 22.8, and 22.8 mg g^{-1} , respectively. Presumably increasing flow rate enables more effective delivery of ions to the less accessible regions of the electrodes, which enhances the mass transportation of the ions and the better utilization of the electrodes, as in RFB systems [34].

Fig. 3b shows the In-situ SAR vs SAC plots of the HCDI setup for the investigated flow rates. Increasing flow rate leads to a substantial increase in both the SAC and the SAR of the system from 5 to 20 mL min^{-1} flow rate. No changes in the SAC and negligible changes in the SAR are recorded when the flow rate is increased from 20 to 40 mL min^{-1} . The most significant outcome is the strong dependence of the initial salt adsorption rate on the flow rate. The trends between the SAC and the SAR show a notable dependence on the flow rate. Slower flow rates (5 and 10 mL min^{-1}) show lower SAR initially (1/10th and half of the 20 mL min^{-1} for 5 and 10 mL min^{-1} , respectively) and lower peak salt adsorption rate (PSAR, 1/3rd and half of the 20 mL min^{-1} for 5 and 10 mL min^{-1} , respectively). Additionally, after PSAR a sharp decrease with increasing SAC is observed rather than a plateau region of SAR. On the other hand, the trends observed in the experiment with flow rates of 20 and 40 mL min^{-1} have comparable performances and show initially high and steady (plateau) SAR values, followed by a sharp decrease due to electrodes reaching saturated state. The trend observed for the salt adsorption kinetics is attributed to increasing flow rate enabling more effective delivery of ions to the electrodes as in flowable Faradaic energy storage systems (i.e. redox flow batteries) [34]. Since no noteworthy salt removal performance improvement is seen at 40 mL min^{-1} , a flow rate of 20 mL min^{-1} is employed to investigate the influences of the cathode thickness and the conductive additive loading in a cathode on the salt removal performance of an HCDI system.

3.4. Effects of cathode thickness on HCDI performance

One of the challenges of the HCDI systems is selecting the proper ratio of the mass of the anode to the cathode. Due to HCDI having an asymmetric setup, if improperly decided whether an anode or a cathode may limit the salt removal performance of the system by causing

underutilization of the other electrode. To overcome this challenge and understand the effect of a cathode thickness on the salt removal performance of the HCDI system, cathodes with different thicknesses (150, 300, 450, 600 μm) have been investigated in this work with the fixed anode thickness (i.e. 500 μm). The purpose of keeping the anode thickness fixed is to see if an anode causes any limitations in salt removal performance via comparing SAC and SAR values for cases containing cathodes of different thickness. Furthermore, by increasing the cathode thickness we aimed to determine the limiting cathode thickness which lets ions to penetrate through the cathode without causing any performance loss. HCDI tests are conducted with the fixed half cycle length (120 min) and flow rate (20 mL min^{-1}) values, while employing MnO_2 cathodes (85 wt% $\alpha\text{-MnO}_2$, 10 wt% CB, 5 wt% PTFE) with varying thicknesses of 150, 300, 450, 600 μm and the ACC anode with a fixed thickness of 500 μm (Zorflex FM50-K). Due to changing the cathode thicknesses, total electrode masses, used to calculate SAC and SAR, vary significantly and are listed in Table 1. By varying the cathode thickness and thus mass of the manganese oxide electrode, insights into the salt removal performance limitations of heavier and thicker electrodes for practical applications can be provided.

Fig. 4a shows the ionic conductivity vs time plots for all investigated cathode thickness cases. Cathodes with thicknesses of 150, 300, 450, and 600 μm have shown SAC values of 22.8, 23.7, 26.1, and 13.1 mg g^{-1} , respectively. These results suggest that up to the cathode thickness of 450 μm , active masses of the electrodes are utilized properly for salt removal, suggesting that the ACC anode is not limiting the salt removal performance of the HCDI system for the cathodes with thicknesses of 150, 300, and 450 μm . However, for the 600 μm thick cathode the performance of HCDI system has decreased substantially (Fig. 4). It should be noted that increasing cathode thickness not only increases the length of penetration path for ions from salty water but also increases the electronic resistance of the poorly conducting oxide electrodes containing polymer binder. Ion transport and electronic conductivity limitations would both increase the likelihood of the underutilization of the cathode and are believed to have caused the sharp decrease in the SAC exhibited by the HCDI cell containing a 600 μm thick cathode.

In-situ SAR vs SAC plots for the tested cathode thicknesses are given in Fig. 4b. The trend between the SAC and the SAR is comparable for the cells containing cathodes with the thicknesses of 150–450 μm . The SAC values show a continuous increase with increasing cathode thickness, while the PSAR values increase from 150 to 450 μm thick cathode, which suggest the presence of more active sites for surface adsorption reactions to take place due to increased amount of MnO_2 nanowires in the thicker electrodes. Yet, the cell containing a 450 μm thick cathode does not show a plateau SAR region, which is observed for the cells containing 150 and 300 μm thick cathodes. This unique behavior seen for the cathode with the thickness of 450 μm is believed to indicate the increasing hindrance of effective ion delivery to the active cathode

mass. But the achieved SAC value suggests that the induced ion transportation limitations are not severe enough to cause an underutilization of the active cathode mass yet, as in the case of the cell containing a 600 μm thick MnO_2 cathode.

However, upon cathode thickness reaching 600 μm , the trend between the SAC and the SAR is changed and the electrodes are seemed to be underutilized for the salt adsorption. Additionally, the cell containing 600 μm thick cathode shows two quarter circles in the corresponding In-situ SAR vs SAC plot, unlike any of the other cases. This unique behavior is interpreted as some of the initially unutilized (or inaccessible) active mass of the 600 μm thick cathode becoming accessible to ions while charging continues. In other words, observing the second plateau region suggests that surface adsorption reactions start again at initially unused regions of the cathode. The significantly lower salt removal performance observed for the cell containing 600 μm thick cathode is attributed to limitations in ion transport and electronic conductivity across the cathode thickness. Since cells containing 150, 300, and 450 μm thick cathodes exhibited comparable salt removal performances, the 150 μm thick cathode has been selected to study the effect of the conductive additive loading in a cathode, to ensure the excess of carbon at an anode side to compensate for the possible increase in the volume-based faradaic processes in $\alpha\text{-MnO}_2$ at a cathode side.

3.5. Effects of conductive additive loading in cathode on HCDI performance

The effects of conductive additive loading in the cathode on the salt removal performance of an HCDI system are investigated using 120 min long half cycles, 20 mL min^{-1} flow rate as the fixed testing parameters, while employing cathodes with 150 μm thickness and the anode with a fixed thickness of 500 μm (Zorflex FM50-K). CB loading in the tested cathodes are 10, 30, and 50 wt% while a polymer binder amount is fixed at 5 wt%. In addition to these compositions, an all CB cathode composed of 95 wt% CB and 5 wt% PTFE is used as a reference to understand the performance increase enabled by faradaic $\alpha\text{-MnO}_2$ electrode component. By varying the conductive additive loading in the cathodes and thus mass of the manganese oxide, insights into the salt removal performance enhancement of more conductive electrodes for practical applications can be provided. Gravimetric normalization of the salt removal performance is done relative to the total masses of the anode and the cathode (including conductive additive and binder, Fig. 5b), same as in the rest of the study. In addition to that, gravimetric normalization of salt removal performance relative to only the active masses of the anode (same for ACC), and the cathode (only the mass of $\alpha\text{-MnO}_2$) are reported to further emphasize the impact of electrode conductivity on the performance of an HCDI system (Fig. 5c).

Electronic conductivity values of 10, 30, and 50 wt% CB loaded cathodes are given in Table 2. As expected, increasing conductive additive loading resulted in the remarkably increased electronic conductivities of the cathodes. Electronic conductivity of the cathodes having 30 wt% and 50 wt% CB loading has increased 13 and 207 fold relative to cathode with 10 wt% CB loading, respectively. Fig. 5a shows the ion concentration vs time plots for the tested cathodes. Increasing the conductive additive loading from 10 to 50 wt% has led to higher SAC values. Cathodes with 10, 30, and 50 wt% CB loading have demonstrated the SAC values of 22.8, 23.7, and 25.4 mg g^{-1} , respectively. It should be noted that all electrodes reached the saturated state. Although increasing the conductive additive loading decreases the amount of active material in the cathode, salt removal performance is observed to have notably increased. This enhancement is attributed to the significant increase in the electronic conductivity of the cathode (see Table 2) leading to the better utilization of the active mass of the cathode for salt removal from the saline water [35].

Increasing SAC with CB loading in a cathode might be considered as the contribution of CB to the salt removal performance. Although CB is reported to show very small SAC due to its very low surface area [2], all

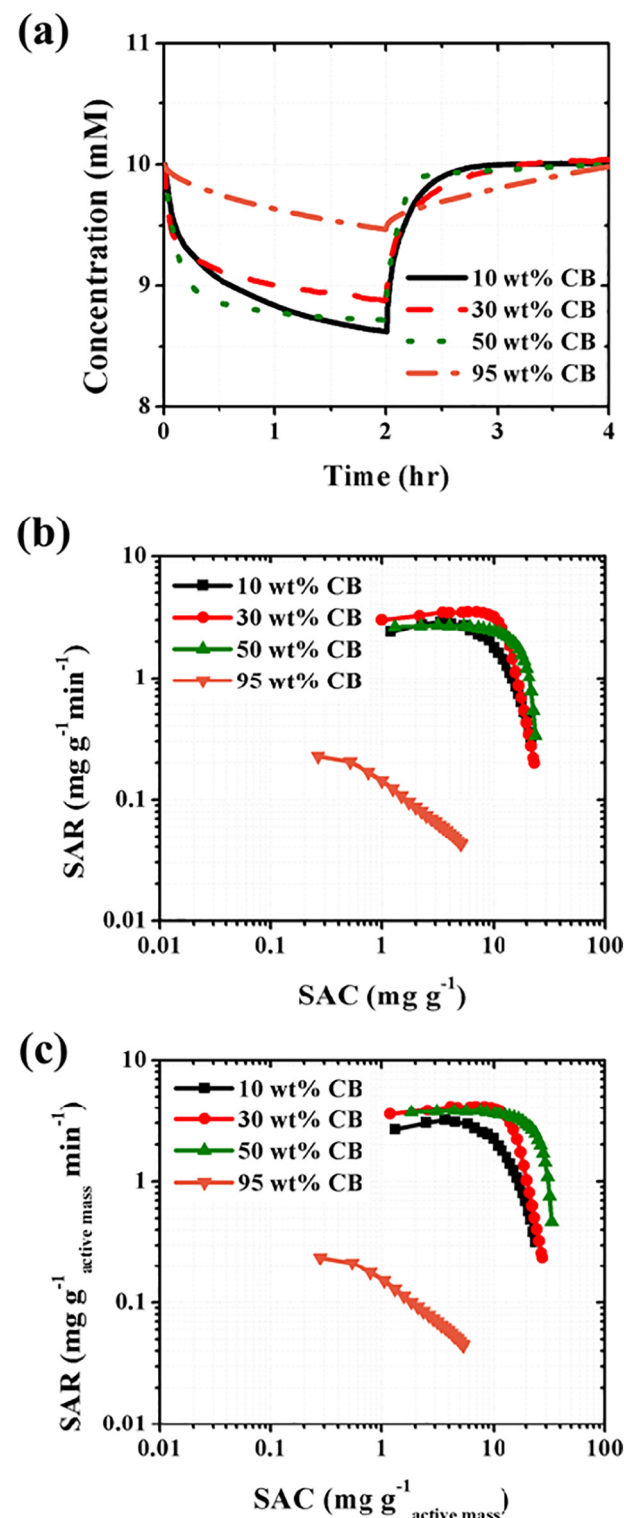


Fig. 5. (a) Concentration vs time graph, (b) in-situ SAR vs SAC plot of the HCDI depending on cathode composition, and (c) in-situ SAR vs SAC plot of the HCDI system for active mass normalization.

CB cathode is prepared and tested with ACC anode using the same conditions as in the cases containing $\alpha\text{-MnO}_2$ cathode to confirm that CB has negligibly small contribution to SAC and negative impact on SAR (Fig. 5b). These results suggest that the performance enhancement seen with increasing CB loading is due to more effective charge transfer as a result of increased electronic conductivity of the cathode. Furthermore, the contribution of CB in the cathode to the salt removal

Table 2

The electronic conductivity of cathodes with varying conductive additive loadings.

Electrode	Electronic conductivity (S m^{-1})
10 wt% CB	0.057 ± 0.012
30 wt% CB	0.738 ± 0.035
50 wt% CB	11.772 ± 4.574
ACC [31]	32.602 ± 0.003

performance metrics is negligibly small.

In-situ SAR vs SAC plot (Fig. 5b) shows the effect of the increased cathode conductivity on overall salt removal performance of the HCDI system. Increasing electronic conductivity does not only increase the SAC but also the PSAR values of the electrodes. In addition, enhanced and longer plateau regions are observed for the SAR values in the In-situ SAR vs SAC plots with increasing electronic conductivity of the cathode. These observations suggest that increasing electronic conductivity of the cathode enables better utilization of both the anode and the cathode, resulting in the HCDI system exhibiting higher salt adsorption capacity and faster kinetics.

To further emphasize the impact of electronic conductivity of the cathode on the salt removal performance of an HCDI system, In-situ SAR vs SAC plots are modified by isolating the mass of the active material in the electrodes for normalization of capacity and rate (Fig. 5c). Calculating the SAC and SAR values by isolating the active electrode masses shows how profoundly the electrode conductivity affects the utilization of the electrodes for salt removal purposes in HCDI systems. SAC values are calculated to be 24.18, 27.89, and 33.80 mg g^{-1} active mass for 10, 30, and 50 wt% CB loaded cathodes, respectively. When CB loading in cathodes has increased from 10 to 50 wt%, the HCDI systems have showed a 40% increase in SAC of the active mass, which highlights the immediate influence of electronic conductivity on the active material in the electrodes. Recorded increase in salt removal performance shows how impactful the electronic conductivity of electrodes is for better utilization of the electrodes for the HCDI applications. These capacity and rate results highlight the importance of effective charge transport across the cathode in HCDI systems, as well as the effective delivery of ions to the electrodes for superior salt removal performance.

3.6. Perspective on the testing conditions

The ACC electrodes (Zorflex FM50-K) employed as an anode is a commonly used material in the traditional CDI research, which shows SAC values around $\sim 2\text{--}5.9 \text{ mg g}^{-1}$ [31,36–38]. However, when ACC is used in an asymmetric setup with a 450 μm thick Faradaic cathode in this study, the SAC exhibited by the HCDI cell reached $\sim 26 \text{ mg g}^{-1}$. The large improvement in salt removal performance is attributed to the high salt adsorption capacity of $\alpha\text{-MnO}_2$. Our results show that the ACC anode can be forced to adsorb more Cl^- ions, for the sake of charge neutrality within the anode and the HCDI cell. Charge neutrality is reached within the cell when each charged species stored in the cathode is neutralized by a species with an opposite charge sign stored in the anode. Also, for charge neutrality within the anode and the cathode, they have to adsorb oppositely charged ions from the saline water (i.e. counter-ion adsorption for non-faradaic EDL electrodes).¹ As a result of the charge neutrality in the system, ACC anodes are believed to be able to adsorb several times the number of Cl^- ions in the asymmetric HCDI setup, as compared to their adsorption ability in a symmetric traditional CDI setup [31,36–38].

Although half cycle length and electrode conductivity results are in good agreement with the trends reported for other CDI systems, the effects of flow rate [23,33] and cathode thickness [23,39] on salt

removal performance are found to show opposite trends than what have been seen for traditional CDI systems. The trend difference observed for flow rates and cathode thicknesses are believed to result from the difference in the nature of charge storage mechanism between traditional CDI (i.e. capacitive EDL) and HCDI (i.e. capacitive EDL and redox active) systems. The trend observed for the flow rates in HCDI system is in good agreement with the flow rate performance trend of RFBs [34]. Increasing flow rate decreases the residence time of the ions in saline water and increases the pressure inside the cell enabling more effective delivery of ions to the electrodes. The pressure drops for each flow rate (5, 10, 20, and 40 mL min^{-1}) is measured to be 1, 2, 4, and 8 psi, respectively. These results are in line with flow rate trend of RFB's reported in literature [34,40].

Furthermore, increasing cathode thickness is reported to decrease both the SAC and the SAR due to increased electronic resistance and ion transport limitations [23]. However, the HCDI system shows an increasing salt adsorption trend with increasing cathode thickness until it reaches 450 μm , followed by a sharp performance decay for the thicker electrodes. We believe that the reason why increasing cathode thickness does not cause immediate performance limitations is the nanowire morphology of the $\alpha\text{-MnO}_2$, which allows for the formation of highly porous electrodes with good wettability enabling efficient penetration of the salty water. Lastly, electronic conductivity is found to strongly affect the salt adsorption capacity and rate of the HCDI system. The profound impact of electronic conductivity on HCDI performance is believed to result from more effective charge transport (with lower loss on the way) across the cathode. Enhanced salt removal performance with increasing CB loading is attributed to increasing electronic conductivity enabling better utilization of active $\alpha\text{-MnO}_2$ mass, with CB contributing negligibly to salt removal performance of the HCDI system.

4. Conclusion

In this study, the effects of half cycle length, flow rate, cathode thickness, and cathode composition on the salt removal performance of an HCDI system were investigated. Overall, the salt removal performance (i.e. SAC and SAR) of the HCDI systems is found to strongly depend on the cell operation conditions and cathode parameters. Increasing half cycle length is observed to improve the SAC while decreasing the PSAR. On the other hand, unlike in traditional CDI systems, increasing flow rate is found to increase the SAC and the PSAR of the HCDI system significantly until the 20 mL min^{-1} flow rate, which can be attributed to the better mass transport of salt species to the electrode surface. Electrochemical testing of the cells with varying cathode thickness and a fixed anode thickness showed that both the SAC and the PSAR values are found to increase and ion diffusion is not limited until the cathode thickness of 450 μm . No sign of the underutilization of the electrodes is noticed until 450 μm cathode thickness. Yet, for the 600 μm thick cathode, both the SAC and the PSAR decreased by 43% and 71%, respectively, suggesting underutilization of electrodes and diffusion limitations. Higher CB loading in the cathodes seems to enable higher salt adsorption capacity and faster rate, due to better utilization of electrodes, resulting from more effective charge transfer across the cathode. Our analyses indicate that in case of HCDI technology, cell design parameters and electrode properties cannot be directly adopted from the traditional CDI and battery experimental setups. More research is sought to establish the standardized parameters for carrying out HCDI experiments in laboratories worldwide to enable direct comparison of the results obtained by different groups. Overall, the results show that the ideal operating conditions for HCDI systems differ greatly from conventional CDI systems due to the inherent contrast between the charge storage mechanisms. In this manner, proper design considerations specific to HCDI systems should be taken to allow achieving highest performance.

¹ Co-ion expulsion is not possible due to the presence of IEM's.

Abbreviations

ACC	Activated Carbon Cloth
HCDI	Hybrid Capacitive Deionization
MCDI	Membrane Capacitive Deionization
SAC	Salt Adsorption Capacity
SAR	Salt Adsorption Rate
PSAR	Peak Salt Adsorption Rate

Author contributions

The manuscript was written through contributions of all authors. All authors have given approval to the final version of the manuscript.

Acknowledgment

E. Pomerantseva acknowledges funding from the National Science Foundation (Grant CMMI-1635233).

E. Caglan Kumbur would like to thank the National Science Foundation (Grant #1351161) for supporting this work.

Appendix A. Supplementary data

Supplementary data to this article can be found online at <https://doi.org/10.1016/j.desal.2018.10.025>.

References

- [1] M.A. Anderson, A.L. Cudero, J. Palma, Capacitive deionization as an electrochemical means of saving energy and delivering clean water. Comparison to present desalination practices: will it compete? *Electrochim. Acta* 55 (2010) 3845–3856.
- [2] S. Porada, R. Zhao, A. van der Wal, V. Presser, P.M. Biesheuvel, Review on the science and technology of water desalination by capacitive deionization, *Prog. Mater. Sci.* 58 (2013) 1388–1442.
- [3] M.E. Suss, S. Porada, X. Sun, P.M. Biesheuvel, J. Yoon, V. Presser, Water desalination via capacitive deionization: what is it and what can we expect from it? *Energy Environ. Sci.* 8 (2015) 2296–2319.
- [4] P.M. Biesheuvel, A. van der Wal, Membrane capacitive deionization, *J. Membr. Sci.* 346 (2010) 256–262.
- [5] J.-B. Lee, K.-K. Park, H.-M. Eum, C.-W. Lee, Desalination of a thermal power plant wastewater by membrane capacitive deionization, *Desalination* 196 (2006) 125–134.
- [6] J. Lee, S. Kim, C. Kim, J. Yoon, Hybrid capacitive deionization to enhance the desalination performance of capacitive techniques, *Energy Environ. Sci.* 7 (2014) 3683–3689.
- [7] B.W. Byles, B. Hayes-Oberst, E. Pomerantseva, Ion removal performance, structural/compositional dynamics, and electrochemical stability of layered manganese oxide electrodes in hybrid capacitive deionization, *ACS Appl. Mater. Interfaces* 10 (2018) 32313–32322.
- [8] B.W. Byles, D.A. Cullen, K.L. More, E. Pomerantseva, Tunnel structured manganese oxide nanowires as redox active electrodes for hybrid capacitive deionization, *Nano Energy* 44 (2018) 476–488.
- [9] M.E. Suss, V. Presser, Water desalination with energy storage electrode materials, *Joule* 2 (2018) 10–15.
- [10] L. Guo, R. Mo, W. Shi, Y. Huang, Z.Y. Leong, M. Ding, F. Chen, H.Y. Yang, A Prussian blue anode for high performance electrochemical deionization promoted by the faradaic mechanism, *Nanoscale* 9 (2017) 13305–13312.
- [11] S. Kim, J. Lee, C. Kim, J. Yoon, Na₂FeP2O₇ as a novel material for hybrid capacitive deionization, *Electrochim. Acta* 203 (2016) 265–271.
- [12] F. Xing, T. Li, J. Li, H. Zhu, N. Wang, X. Cao, Chemically exfoliated MoS₂ for capacitive deionization of saline water, *Nano Energy* 31 (2017) 590–595.
- [13] J. Lee, P. Srimuk, K. Aristizabal, C. Kim, S. Choudhury, Y.-C. Nah, F. Mücklich, V. Presser, Pseudocapacitive desalination of brackish water and seawater via vanadium pentoxide decorated multi-walled carbon nanotubes, *ChemSusChem* 10 (18) (2017) 3611–3623.
- [14] Y.-H. Liu, H.-C. Hsi, K.-C. Li, C.-H. Hou, Electrodeposited manganese dioxide/activated carbon composite as a high-performance electrode material for capacitive deionization, *ACS Sustain. Chem. Eng.* 4 (2016) 4762–4770.
- [15] S. Hand, R.D. Cusick, Characterizing the impacts of deposition techniques on the performance of MnO₂ cathodes for sodium electro sorption in hybrid capacitive deionization, *Environ. Sci. Technol.* 51 (2017) 12027–12034.
- [16] H. Yoon, J. Lee, S. Kim, J. Yoon, Hybrid capacitive deionization with Ag coated carbon composite electrode, *Desalination* 422 (2017) 42–48.
- [17] P. Srimuk, F. Kaasik, B. Krüner, A. Tolosa, S. Fleischmann, N. Jäckel, M.C. Tekeli, M. Aslan, M.E. Suss, V. Presser, MXene as a novel intercalation-type pseudocapacitive cathode and anode for capacitive deionization, *J. Mater. Chem. A* 4 (2016) 18265–18271.
- [18] M. Pasta, C.D. Wessells, Y. Cui, F. La Mantia, A desalination battery, *Nano Lett.* 12 (2012) 839–843.
- [19] P. Srimuk, J. Lee, S. Fleischmann, S. Choudhury, N. Jäckel, M. Zeiger, C. Kim, M. Aslan, V. Presser, Faradaic deionization of brackish and sea water via pseudo-capacitive cation and anion intercalation into few-layered molybdenum disulfide, *J. Mater. Chem. A* 5 (2017) 15640–15649.
- [20] K.C. Smith, R. Dmello, Na-ion desalination (NID) enabled by Na-blocking membranes and symmetric Na-intercalation: porous-electrode modeling, *J. Electrochem. Soc.* 163 (2016) A530–A539.
- [21] T. Kim, C.A. Gorski, B.E. Logan, Low energy desalination using battery electrode deionization, *Environ. Sci. Technol. Lett.* 4 (2017) 444–449.
- [22] S.A. Hawks, A. Ramachandran, S. Porada, P.G. Campbell, M.E. Suss, P.M. Biesheuvel, J.G. Santiago, M. Stadermann, Performance Metrics for the Objective Assessment of Capacitive Deionization Systems, (2018).
- [23] T. Kim, J. Yoon, CDI ragone plot as a functional tool to evaluate desalination performance in capacitive deionization, *RSC Adv.* 5 (2015) 1456–1461.
- [24] R. Zhao, O. Satpradit, H. Rijnarts, P. Biesheuvel, A. Van der Wal, Optimization of salt adsorption rate in membrane capacitive deionization, *Water Res.* 47 (2013) 1941–1952.
- [25] S. Porada, L. Borchardt, M. Oschatz, M. Bryjak, J.S. Atchison, K.J. Keesman, S. Kaskel, P.M. Biesheuvel, V. Presser, Direct prediction of the desalination performance of porous carbon electrodes for capacitive deionization, *Energy Environ. Sci.* 6 (2013) 3700–3712.
- [26] E.J. Post, Manganese oxide minerals: crystal structures and economic and environmental significance, *Proc. Natl. Acad. Sci. U. S. A.* 96 (1999) 3447–3454.
- [27] Y. Gao, Z. Wang, J. Wan, G. Zou, Y. Qian, A facile route to synthesize uniform single-crystalline MnO₂ nanowires, *J. Cryst. Growth* 279 (2005) 415–419.
- [28] P.M. Biesheuvel, R. Zhao, S. Porada, A. van der Wal, Theory of membrane capacitive deionization including the effect of the electrode pore space, *J. Colloid Interface Sci.* 360 (2011) 239–248.
- [29] A.S. Poyraz, J. Huang, S. Cheng, L. Wu, X. Tong, Y. Zhu, A.C. Marschilok, K.J. Takeuchi, E.S. Takeuchi, Tunnel structured α -MnO₂ with different tunnel cations (H⁺, K⁺, Ag⁺) as cathode materials in rechargeable Lithium batteries: the role of tunnel cation on electrochemistry, *J. Electrochem. Soc.* 164 (2017) A1983–A1990.
- [30] B.W. Byles, N.K.R. Palapati, A. Subramanian, E. Pomerantseva, The role of electronic and ionic conductivities in the rate performance of tunnel structured manganese oxides in Li-ion batteries, *APL Mater.* 4 (2016) 046108.
- [31] L. Agartan, B. Akuzum, T. Mathis, K. Ergenekon, E. Agar, E.C. Kumbur, Influence of thermal treatment conditions on capacitive deionization performance and charge efficiency of carbon electrodes, *Sep. Purif. Technol.* 202 (2018) 67–75.
- [32] C. Zhao, G. Liu, N. Sun, X. Zhang, G. Wang, Y. Zhang, H. Zhang, H. Zhao, Biomass-derived N-doped porous carbon as electrode materials for Zn-air battery powered capacitive deionization, *Chem. Eng. J.* 334 (2017) 1270–1280.
- [33] M. Mossad, L. Zou, A study of the capacitive deionisation performance under various operational conditions, *J. Hazard. Mater.* 213–214 (2012) 491–497.
- [34] C.R. Dennison, E. Agar, B. Akuzum, E.C. Kumbur, Enhancing mass transport in redox flow batteries by tailoring flow field and electrode design, *J. Electrochem. Soc.* 163 (2016) A5163–A5169.
- [35] R. Jiang, C. Cui, H. Ma, Using graphene nanosheets as a conductive additive to enhance the capacitive performance of α -MnO₂, *Electrochim. Acta* 104 (2013) 198–207.
- [36] K. Laxman, M.T. Myint, H. Bourdoucen, J. Dutta, Enhancement in ion adsorption rate and desalination efficiency in a capacitive deionization cell through improved electric field distribution using electrodes composed of activated carbon cloth coated with zinc oxide nanorods, *ACS Appl. Mater. Interfaces* 6 (2014) 10113–10120.
- [37] K. Laxman, M.T.Z. Myint, R. Khan, T. Pervez, J. Dutta, Improved desalination by zinc oxide nanorod induced electric field enhancement in capacitive deionization of brackish water, *Desalination* 359 (2015) 64–70.
- [38] M.-W. Ryoo, G. Seo, Improvement in capacitive deionization function of activated carbon cloth by titania modification, *Water Res.* 37 (2003) 1527–1534.
- [39] S. Porada, M. Bryjak, A. van der Wal, P.M. Biesheuvel, Effect of electrode thickness variation on operation of capacitive deionization, *Electrochim. Acta* 75 (2012) 148–156.
- [40] J. Houser, J. Clement, A. Pezeski, M.M. Mench, Influence of architecture and material properties on vanadium redox flow battery performance, *J. Power Sources* 302 (2016) 369–377.